USGS
science for a changing world

Overview of the Geologic Effects of the November 14, 2016, M_w 7.8 Kaikoura, New Zealand, Earthquake

Scientific Investigations Report 2017–5146

U.S. Department of the Interior
U.S. Geological Survey

Cover. Photograph showing the main scarp and upper part of the Sea Front landslide. (See fig. 1*D*.)

Overview of the Geologic Effects of the November 14, 2016, M_w 7.8 Kaikoura, New Zealand, Earthquake

By Randall W. Jibson, Kate E. Allstadt, Francis K. Rengers, and Jonathan W. Godt

Scientific Investigations Report 2017–5146

U.S. Department of the Interior
U.S. Geological Survey

U.S. Department of the Interior
RYAN K. ZINKE, Secretary

U.S. Geological Survey
William H. Werkheiser, Deputy Director
exercising the authority of the Director

U.S. Geological Survey, Reston, Virginia: 2018

Suggested citation:
Jibson, R.W., Allstadt, K.E., Rengers, F.K., and Godt, J.W., 2018, Overview of the geologic effects of the November 14, 2016, M_w 7.8 Kaikoura, New Zealand, earthquake: U.S. Geological Survey Scientific Investigations Report 2017–5146, 39 p., https://doi.org/10.3133/sir20175146.

ISSN 2328-0328 (online)

Acknowledgments

GNS Science, New Zealand, hosted this reconnaissance trip and provided both logistical support and data sharing for this effort; Chris Massey of GNS Science was the principal cooperator in this effort. Brian Collins of the U.S. Geological Survey and Chris Massey of GNS Science provided thorough and thoughtful reviews of the manuscript.

Contents

Figures

Conversion Factors

International System of Units to U.S. customary units

Multiply	By	To obtain
	Length	
meter (m)	3.281	foot (ft)
kilometer (km)	0.6214	mile (mi)
	Area	
square meter (m^2)	10.76	square foot (ft^2)
square kilometer (km^2)	0.3861	square mile (mi^2)
	Volume	
cubic meter (m^3)	1.308	cubic yard (yd^3)

Datum

Vertical coordinate information is referenced to the New Zealand Vertical Datum 2016 (NZVD2016).

Horizontal coordinate information is referenced to the New Zealand Geodetic Datum 2000 (NZGD2000).

Altitude, as used in this report, refers to distance above the vertical datum.

Abbreviations

g	acceleration of gravity
GNS Science	Institute of Geological and Nuclear Science Limited (New Zealand)
GPS	Global Positioning System
InSAR	interferometric synthetic aperture radar
M_w	earthquake moment magnitude
PGA	peak ground acceleration
PGV	peak ground velocity
SH1	State Highway 1
SIMT	South Island Main Trunk (rail line)
USGS	U.S. Geological Survey
UTC	coordinated universal time

Overview of the Geologic Effects of the November 14, 2016, M_w 7.8 Kaikoura, New Zealand, Earthquake

By Randall W. Jibson, Kate E. Allstadt, Francis K. Rengers, and Jonathan W. Godt

Abstract

The November 14, 2016, Kaikoura, New Zealand, earthquake (moment magnitude [M_w] 7.8) triggered more than 10,000 landslides over an area of about 12,000 square kilometers in the northeastern part of the South Island of New Zealand. In collaboration with GNS Science (the Institute of Geological and Nuclear Science Limited), we conducted ground and helicopter reconnaissance of the affected areas and assisted in rapid hazard evaluation. The majority of the triggered landslides were shallow- to moderate-depth (1–10 meters), highly disrupted falls and slides in rock and debris from Lower Cretaceous graywacke sandstone in the Seaward Kaikoura Range. Deeper, more coherent landslides in weak Upper Cretaceous to Neogene sedimentary rock also were numerous in the gentler topography south and inland (west) of the Seaward Kaikoura Range. The principal ground-failure hazards from the earthquake were the hundreds of valley-blocking landslides, many of which impounded lakes and ponds that posed potential downstream flooding hazards. Both large and small landslides also blocked road and rail corridors in many locations, including the main north-south highway (State Highway 1), which was still closed in October 2017. As part of our investigation, we compared post-earthquake field observations to the output of models used to estimate near-real-time landslide probabilities following earthquakes. The models generally over-predicted landslide occurrence and thus need further refinement.

Introduction

On November 14, 2016, a large (moment magnitude [M_w] 7.8) earthquake struck the northeastern part of the South Island of New Zealand (fig. 1). Named after the coastal town near the epicenter, the Kaikoura earthquake had associated surface rupture on more than 20 mapped faults (Stirling and others, 2017), caused widespread crustal deformation (both uplift and subsidence), and triggered more than 10,000 landslides in the complex topography of the affected area (Dellow and others, 2017). Two fatalities (not related to landslides) were reported, and damage to roads, railways, and other infrastructure was extensive. The two primary transportation routes on the northern part of the South Island—State Highway 1 (SH1) and the South Island Main Trunk (SIMT) rail line—were extensively damaged by faulting, landslides, and tectonic deformation. As of December 2016, direct economic losses are estimated at $2–3 billion NZD ($1.4–2.2 billion USD) (New Zealand Treasury, 2016); this number is likely to increase as more detailed economic data are collected.

In the hours after the earthquake, the U.S. Geological Survey (USGS) informed GNS Science (the Institute of Geological and Nuclear Sciences Limited, the New Zealand Crown Research Institute responsible for earth and natural hazards research) of the availability of satellite imagery over the affected area that was collected soon after the earthquake. Early assessment of the extent and severity of landsliding prompted an informal request from GNS Science for USGS assistance in the evaluation of landslide dams and field verification of landslide mapping. A formal invitation for the USGS to participate in landslide field investigations was received on November 22, 2016. We arrived in New Zealand on December 2, 2016, and departed on December 16, 2016.

Prior to our field visit, we obtained high-resolution satellite imagery (DigitalGlobe, 2016) covering most of the affected area for use in the field. Additionally, several organizations that had begun compiling landslide inventories using this and other satellite imagery soon after the earthquake made them available to us. To help prioritize our field work, we primarily used a point inventory compiled by Valkaniotis and others (2016) and a preliminary version of a polygon inventory compiled by Rathje and others (in press). Rathje and others (2017) subsequently published a completed inventory.

We conducted both ground and aerial reconnaissance. For both types of reconnaissance, we used Global Positioning System (GPS) tracking at approximately 5-meter (m) resolution (fig. 2). Ground surveys were conducted using a four-wheel-drive vehicle and handheld cameras, but they were limited to the edges of the affected area because existing road access to the most affected area was limited and commonly blocked by landslides. Aerial reconnaissance was by helicopter, in which we used both handheld cameras and a GoPro video camera mounted to the helicopter.

Our primary mission was to assist GNS Science in reconnaissance and preliminary hazard evaluation of landslides blocking river channels and of areas where

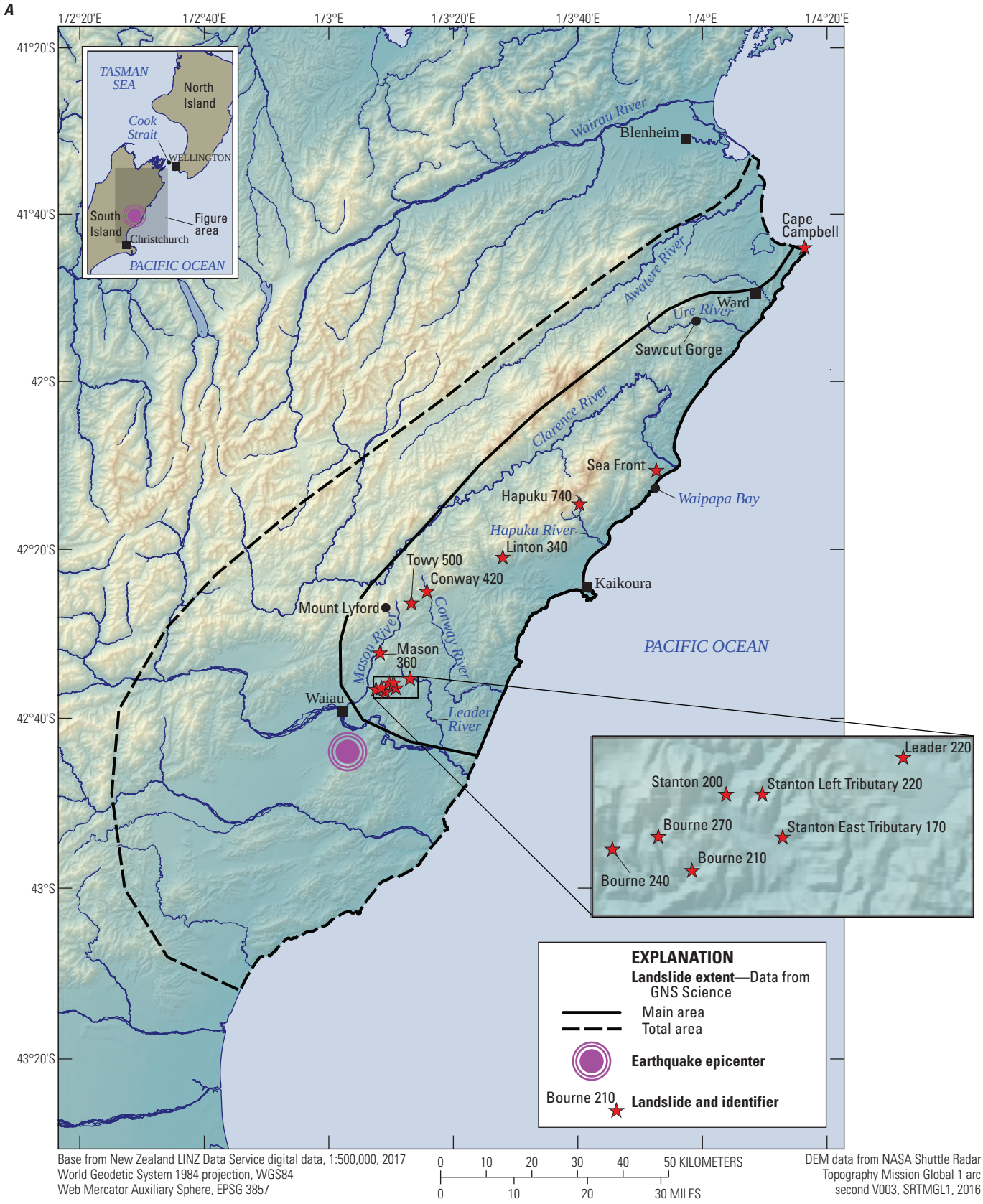

Figure 1. Maps showing earthquake epicenter and landslide area of the 2016 Kaikoura, New Zealand, earthquake and locations of photographs in subsequent figures. *A*, Landslide extent in relation to epicenter and locations of landslides discussed in this report. (Landslide extent from Dellow and others, 2017.)

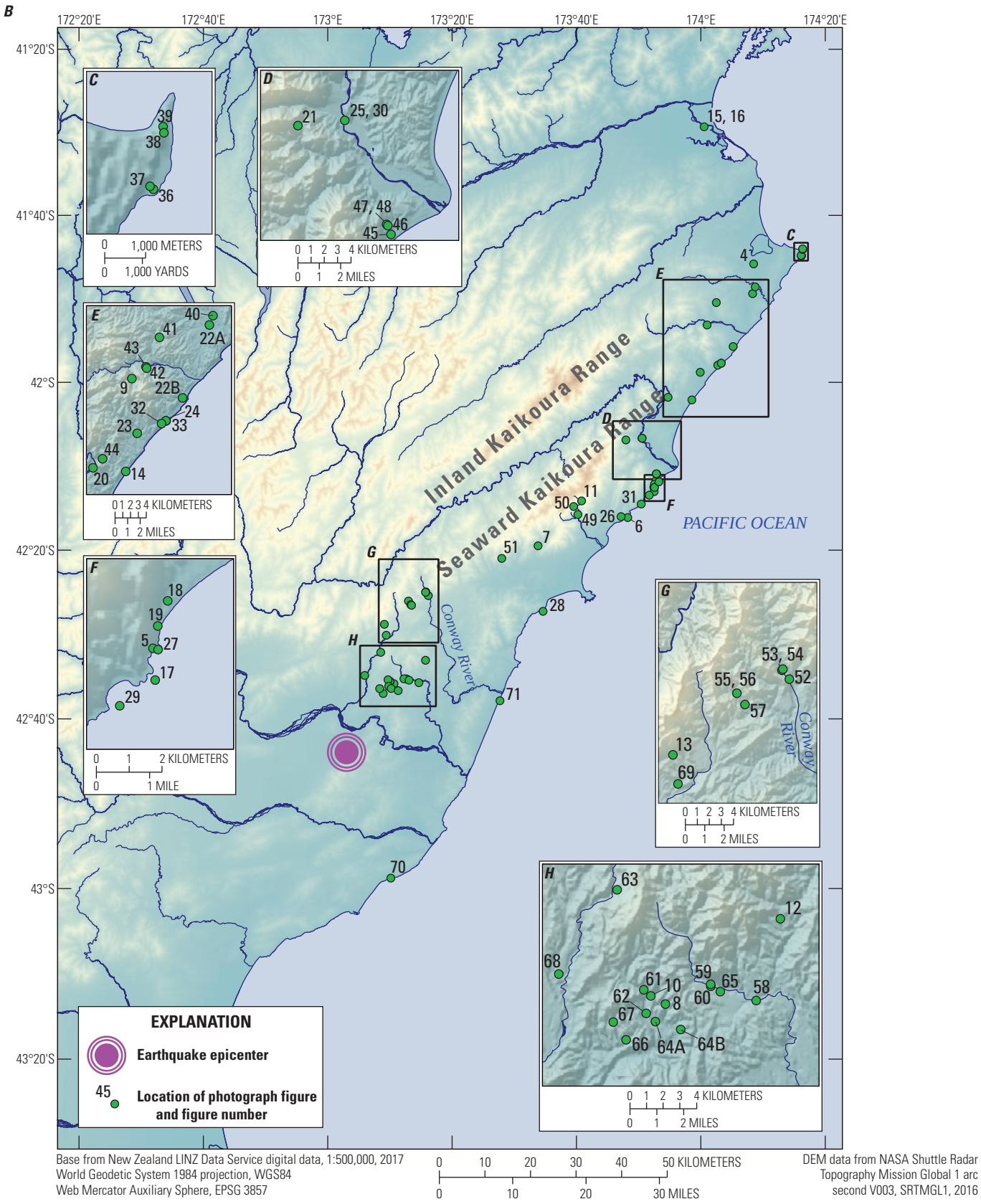

Figure 1. Maps showing earthquake epicenter and landslide area of the 2016 Kaikoura, New Zealand, earthquake and locations of photographs in subsequent figures. *B*, Locations of photographs in Figures 4, 6, 7, 11, 15, 16, 26, 28, 31, 49–51, 70, 71. *C*, Figures 36–39. *D*, Figures 21, 25, 30, 45–48. *E*, Figures 9, 14, 20, 22–24, 32, 33, 40–44. *F*, Figures 5, 17–19, 27, 29. *G*, Figures 13, 52–57, 69. *H*, Figures 8, 10, 12, 58–68.—Continued

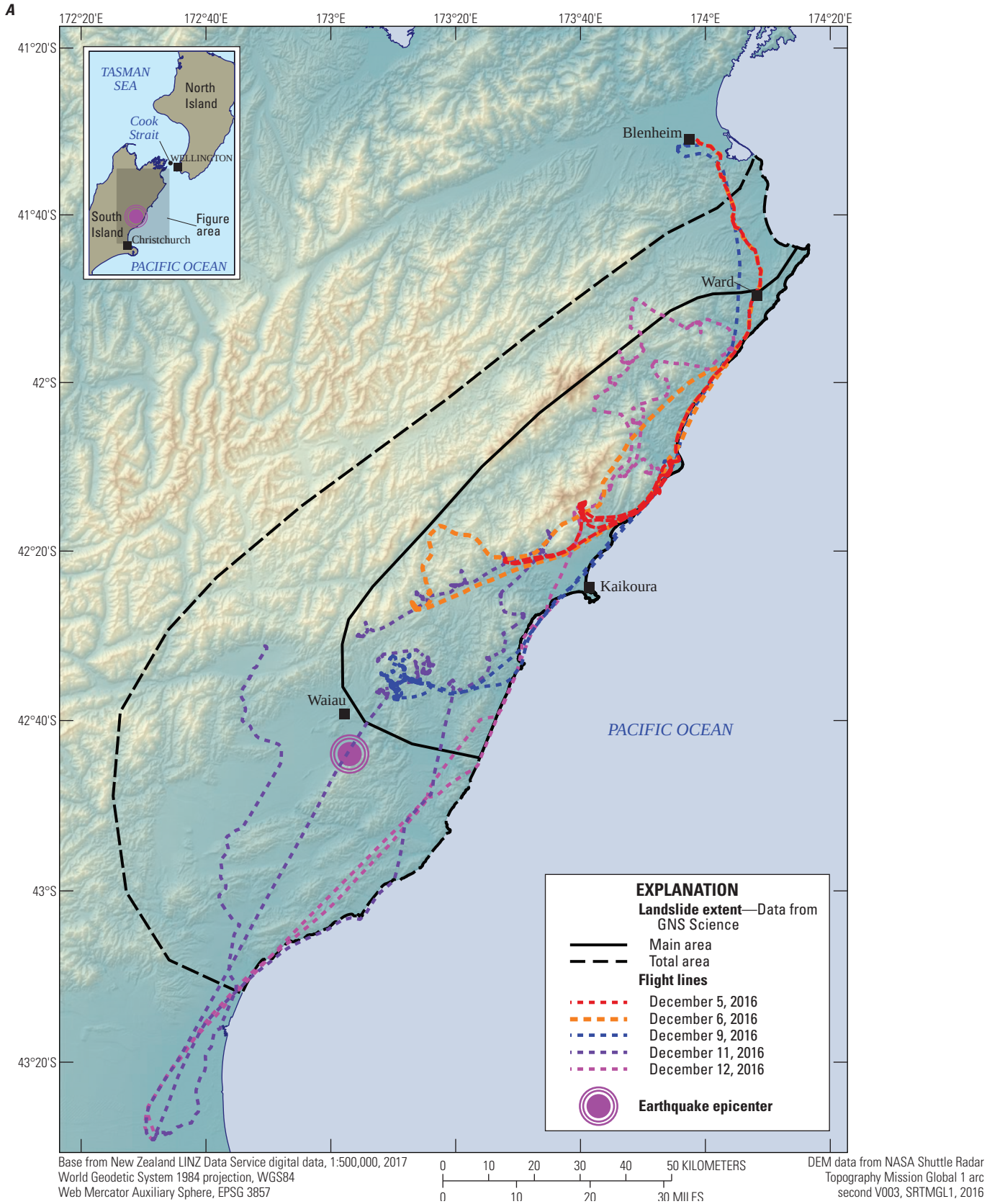

Figure 2. Maps showing daily Global Positioning System tracks for reconnaissance following the 2016 Kaikoura, New Zealand, earthquake. (Landslide extent from Dellow and others, 2017.) *A*, Aerial reconnaissance.

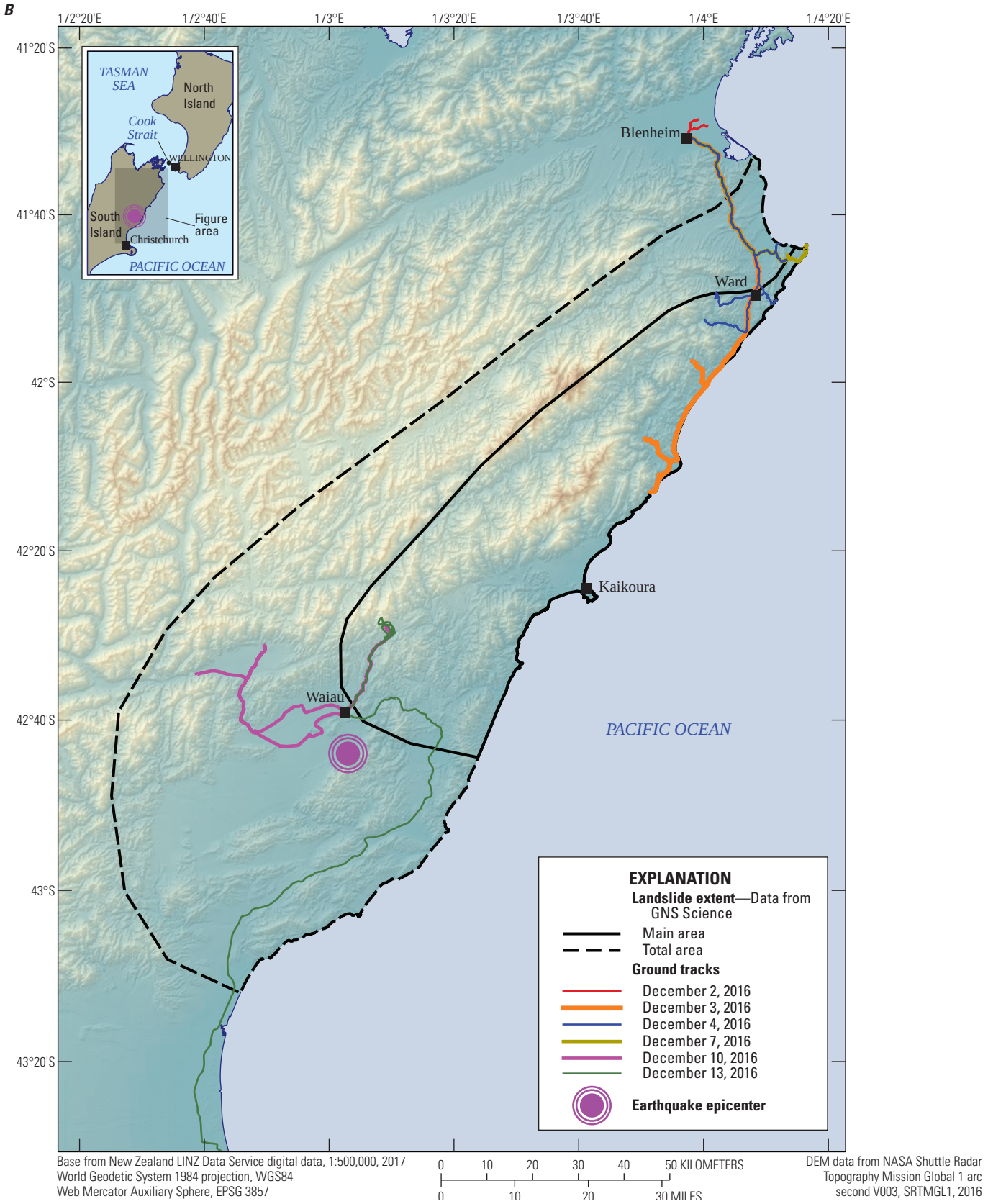

Figure 2. Maps showing daily Global Positioning System tracks for reconnaissance following the 2016 Kaikoura, New Zealand, earthquake. (Landslide extent from Dellow and others, 2017.) *B*, Ground reconnaissance.—Continued

abundant or large landslides had occurred. An additional purpose was to evaluate the quality of several predictive models of ground failure. We also observed surface fault rupture and crustal deformation such as uplift and subsidence. The objective of this report is to summarize preliminary observations of the geologic effects of this earthquake made in site visits and overflights during our visit. This report is preliminary; GNS Science continues to conduct more detailed and quantitative studies.

In this report, we describe the earthquake and provide an overview of all geologic effects observed: landsliding, faulting, and tectonic deformation (uplift and subsidence). We briefly discuss how they affected people and infrastructure, with more detailed field observations and additional photographs of earthquake-related phenomena included in an appendix. We also assess how our field observations compare with estimated landslide distributions predicted by two near-real-time models.

The 2016 Kaikoura, New Zealand, Earthquake

The M_w 7.8 Kaikoura earthquake occurred at 11:02:56 UTC (coordinated universal time) on November 13, 2016 (just after midnight on November 14 local time). The USGS located the epicenter at a depth of 15.2±3.2 kilometers (km) at lat 42.736°S., long 173.050°E. (±4.6 km), about 9 km south of the town of Waiau, New Zealand (U.S. Geological Survey, 2017c). The rupture propagated about 170 km along the northeastern side of the South Island, continued offshore into Cook Strait, and stopped just south of the North Island about 60 km from the capital city of Wellington (Hamling and others, 2017). The earthquake ruptured at least 12 major faults (>1 m offset) and 20 total faults having widely varying strikes, slip styles, and slip amounts; the greatest slips occurred in the area about 80 to 120 km northeast of the epicenter (Litchfield and others, 2017) (fig. 3). Both the USGS finite-fault inversion, based on global seismic data (U.S. Geological Survey, 2017a), and a slip distribution, based on inversions of geodetic and coastal uplift data (Hamling and others, 2017), estimate greater slip at depth around that area.

GeoNet (www.geonet.org.nz) operates strong-motion stations throughout the affected area (fig. 3) and makes the data publicly available. Only one strong-motion station (KEKS, Kekerengu Valley Road) is located in the mountainous area most affected by landsliding. This station is located on a foothill in the northeastern end of the area most affected by landslides, just 3 km from the Kekerengu fault. Some of the greatest lateral surface fault displacements were measured in this area (Litchfield and others, 2017). At this site, horizontal ground accelerations reached 1.2 g (acceleration of gravity), and vertical accelerations reached 0.4 g. Greater ground motions were recorded at two other stations located in low-lying areas on soft soils that likely experienced site amplification: WTMC (Te Mara Farm Waiau) in the Humps fault zone about 13 km from the epicenter (1.1 g horizontal, 3.1 g vertical) and WDFS (Ward Fire Station) in Ward at the northeast end of the affected area, about 6 km from the offshore Needles fault (1.3 g horizontal, 1.2 g vertical).

The USGS produces spatial estimates of ground shaking through a tool called ShakeMap (Wald and others, 1999, 2005; U.S. Geological Survey, 2017d). ShakeMap combines data from felt reports and instrumental recordings such as those provided by GeoNet with ground-motion prediction equations and fault-plane location estimates to create a spatial estimate of several ground-motion parameters such as peak ground acceleration (PGA), peak ground velocity (PGV), and spectral acceleration. Because ShakeMap incorporates new information as it becomes available, the estimated ground motions for this earthquake evolved throughout the study period. Version 16 is the most recent update at the time of this writing (March 2017); this version includes better defined fault planes and more strong-motion data than previous versions. Figure 3 shows estimated PGA values from version 16. ShakeMap version 7 was available when we were in the field, and it provided the ground-motion input for the suite of prototype coseismic landslide and liquefaction prediction models (Allstadt and others, 2016) we used to guide some of our ground investigations (see "Comparison of Observed to Modeled Landslide Distribution" section, p. 16).

As of December 12, 2016, GeoNet reported 8,735 aftershocks, 52 of them M_w 5 and greater (GeoNet, 2016a), strong enough to trigger additional landslides. A M_w 5.5 aftershock occurred while we were driving on SH1 near Ward on December 4, 2016, and we encountered fresh rock falls from several road cuts that were triggered by that event (fig. 4). These rock falls all occurred from slopes that had produced landslides in the main shock.

Figure 3 (following page). Map showing ground shaking from the 2016 Kaikoura, New Zealand, earthquake in relation to the landslide area. (GeoNet sites: AMBC, Amberly; ASHS, Ashley School; BTWS, Nelson Brightwater; BWRS, Waikakaho Road; CACS, Christchurch Canterbury Aero Club; CECS, Cheviot Emergency Centre; CSTC, Cust School; CULC, Culverdon Airlie Farm; GLWS, Glyn Wye; GVZ, Greta Valley; HSES, Manmer Springs Emergency Centre; KEKS, Kekerengu Valley Road; KIKS, Kaikoura; KPOC, Kaiapoi North School; MATS, Matariki Wadsworth Road; MCAS, Murchison Area School; MGCS, Blenheim Marlborough Girls College; MOLS, Molesworth Station; OHSS, Ouruhika School; SCAC, Scargill; SEDS, Seddon Fire Station; SMHS, Summerhill; SWNC, Swannanoa School; THZ, Top House; WAKC, Waikari; WDFS, Ward Fire Station; WIGC, Waiau Gorge; WTMC, Te Mara Farm Waiau; WVFS, Wairau Valley Farm)

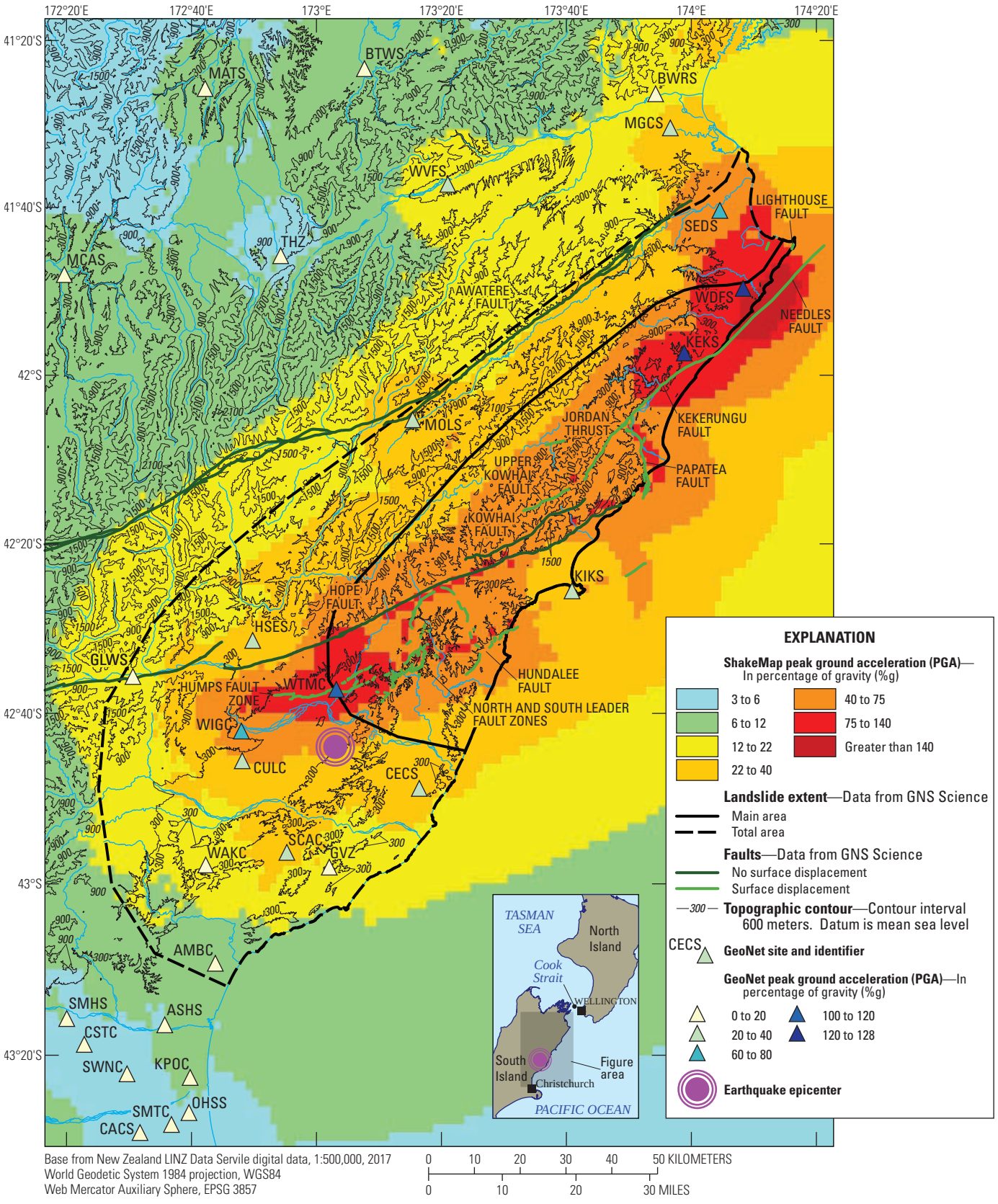
172°20'E
172°40'E
173°E
173°20'E
173°40'E
174°E
174°20'E
41°20'S
41°40'S
42°S
42°20'S
42°40'S
43°S
43°20'S
BTWS
MATS
BWRS
MGCS
WVFS
LIGHTHOUSE FAULT
SEDS
THZ
MCAS
AWATERE FAULT
WDFS
NEEDLES FAULT
KEKS
MOLS
JORDAN THRUST
KEKERUNGU FAULT
UPPER KOWHAI FAULT
PAPATEA FAULT
KOWHAI FAULT
KIKS
HOPE FAULT
HSES
GLWS
HUMPS FAULT ZONE
WTMC
HUNDALEE FAULT
NORTH AND SOUTH LEADER FAULT ZONES
WIGC
CULC
CECS
SCAC
GVZ
WAKC
AMBC
SMHS
ASHS
CSTC
SWNC
KPOC
SMTC
OHSS
CACS
TASMAN SEA
North Island
Cook Strait
WELLINGTON
South Island
Figure area
Christchurch
PACIFIC OCEAN
EXPLANATION
ShakeMap peak ground acceleration (PGA)—In percentage of gravity (%g)
3 to 6
6 to 12
12 to 22
22 to 40
40 to 75
75 to 140
Greater than 140
Landslide extent—Data from GNS Science
Main area
Total area
Faults—Data from GNS Science
No surface displacement
Surface displacement
300 Topographic contour—Contour interval 600 meters. Datum is mean sea level
CECS GeoNet site and identifier
GeoNet peak ground acceleration (PGA)—In percentage of gravity (%g)
0 to 20
20 to 40
60 to 80
100 to 120
120 to 128
Earthquake epicenter
Base from New Zealand LINZ Data Servile digital data, 1:500,000, 2017
World Geodetic System 1984 projection, WGS84
Web Mercator Auxiliary Sphere, EPSG 3857
0 10 20 30 40 50 KILOMETERS
0 10 20 30 MILES

Overview of Geologic Effects of the Kaikoura Earthquake

Landslides

Landslides were the most numerous and widespread effect of the earthquake. We saw thousands of landslides during our reconnaissance, and we estimate that the total number of landslides triggered is more than 10,000. GNS Science initially estimated that the earthquake triggered more than 80,000 landslides over an area of about 12,000 square kilometers (km^2) (GeoNet, 2016b). Subsequent estimates are lower, but the process of creating a comprehensive inventory is ongoing. Not all triggered landslides will be resolvable from satellite imagery, and the true total number of landslides is likely more than what will be recorded in the inventory. Previous studies of worldwide earthquakes have related earthquake magnitude to number of landslides. For a M_w 7.8 earthquake, the relation of Malamud and others (2004) predicts about 25,000 landslides; Keefer's (2002) relation predicts about 60,000 landslides. Both relations are based solely on magnitude and do not take into account other factors (such as earthquake depth, distance to fault, topography, rock type, climate, and vegetation) that contribute. Based on our observations, we judge that the total number of landslides from this earthquake is probably toward the lower end of this range.

The area affected by landslides (approx. 12,000 km^2 as estimated from satellite imagery and regional air and ground reconnaissance) is smaller than predicted by Keefer (1984, 2002); his maximum area for M_w 7.8 is about 90,000 km^2, and the average predicted area is about 22,000 km^2. The outermost extent of landsliding was not mapped during our field reconnaissance, in the GNS Science assessment, or in the other inventories used; we focus on areas where significant concentrations of landslides are present.

Consistent with observations from other worldwide earthquakes (Keefer, 1984, 2002), the large majority of

Figure 4. Photograph showing debris from a road cut that was shaken during the M_w 5.5 aftershock of December 4, 2016, following the 2016 Kaikoura, New Zealand, earthquake. (See fig. 1*B*.)

Figure 5. Photograph showing a small rock fall along State Highway 1 near Waipapa Bay. (See fig. 1*F*.)

Figure 6. Photograph showing a debris slide along State Highway 1 about 14 kilometers southwest of Waipapa Bay. (See fig. 1*B*.)

Figure 7. Photograph showing landslides in the Seaward Kaikoura Range. (See fig. 1*B*.)

triggered landslides are disrupted slides and falls in rock and debris (terminology from Varnes, 1978) of shallow to moderate depth (1–10 m). These types of slides range in size from small features having volumes of a few cubic meters (fig. 5) to larger, deeper landslides having volumes of tens of thousands of cubic meters (fig. 6). Such landslides are pervasive in many parts of the Seaward Kaikoura Range (fig. 7) and the complex topography along the coastline where the slopes are formed mainly in Lower Cretaceous graywacke sandstones and Quaternary sediment.

The earthquake also triggered dozens of large, deep slumps and block slides, which remained much more coherent (terminology from Keefer, 1984). These slides were triggered primarily in weaker Upper Cretaceous to Neogene sedimentary rock and Quaternary sediment (primarily terrace sand and gravel) in the lower, seaward reaches south and west of Kaikoura (fig. 8), where topography is less rugged than in the Seaward Kaikoura Range. Many of these deeper landslides blocked valleys and dammed rivers and posed potential hazards to areas downstream. These types of landslides have volumes in the hundreds of thousands to millions of cubic meters.

The most significant post-earthquake hazard is the formation of landslide dams. GNS Science mapped 196 such dams from satellite imagery, and we saw several hundred dams of all sizes during our aerial reconnaissance. GNS Science named the significant landslide dams by their drainage and approximate elevation in meters above sea level; for example, the Leader 220 landslide dam is in the Leader River drainage at 220 meters above sea level. We use their names in this report. A significant landslide dam is defined as being greater than 10 m high and one whose failure could lead to a flood affecting people or infrastructure downstream. Dams too small to be detected on imagery are abundant in the upper reaches of many drainages, some of which are almost entirely filled with landslide debris (fig. 9). The larger landslide dams impound lakes big enough to pose downstream hazards in the event of sudden breach (fig. 10). Some of the large landslide dams consist of disrupted rock-fall deposits from the steep Lower Cretaceous graywacke slopes (fig. 11); others formed as large, deep block slides in Neogene sedimentary rock that dammed and pinched streams and in some cases entire river valleys (see fig. 10).

Figure 8. Photograph showing the Stanton Left Tributary 220 landslide. (See fig. 1*H*.)

Figure 10. Photograph showing the Leader 220 landslide dam. (See fig. 1*H*.)

Figure 9. Photograph showing landslide debris blocking a channel in Sawcut Gorge. (See fig. 1*E*.)

Figure 11. Photograph showing the Hapuku 740 landslide dam. (See fig. 1*B*.)

Ground Cracking

Ground cracking was widespread following the earthquake. Cracks on steep slopes appear to be gravitationally influenced and to relate to incipient landsliding (fig. 12). Likewise, cracks along the outboard edges of roads excavated into steep slopes (fig. 13) are common and probably relate to incipient sliding or slumping in fill material along the edge of the road as well as possible amplification of ground shaking at steep breaks in slope (Ashford and others, 1997). Other cracks appear unrelated to topography and probably resulted from strong ground shaking (fig. 14). Topographic noses (spur ends) at the ends of ridges experienced extensive cracking, probably related to topographic amplification of ground shaking; such concentration of cracking on the ends of ridges has been observed in previous earthquakes (Keefer and Manson, 1998; Collins and Jibson, 2015).

Liquefaction

We observed evidence of liquefaction in several areas near the mouth of the Wairau River northeast of Blenheim (fig. 1). The liquefied deposits are in Quaternary alluvial and estuarine sand and silt along the main river channel and its distributaries. Evidence of liquefaction includes numerous deposits of ejected sand and silt in several areas (fig. 15) as well as lateral-spread landslides along river channels. Lateral spreads formed primarily parallel to and within a few hundred meters of river banks (fig. 16). Lateral-spread displacements ranged up to a few meters. Liquefaction from this earthquake was documented more extensively by the team supported by Geotechnical Extreme Events Reconnaissance (GEER, 2017).

Figure 12. Photograph showing ground cracking on a hillside near Conway River. (See fig. 1*H*.)

Figure 14. Photograph showing ground cracks unrelated to slope failure. (See fig. 1*E*.)

Figure 13. Photograph showing cracks along the outboard edge of a mountain road above Mount Lyford. (See fig. 1*G*.)

Figure 15. Photograph showing ejected sand near the Wairau River northeast of Blenheim. (See fig. 1*B*.)

Figure 16. Photograph showing lateral spread along the Wairau River northeast of Blenheim. (See fig. 1*B*.)

Figure 17. Photograph showing surface fault rupture along the Papatea fault (indicated by black arrows) extending through the source area of the Sea Front landslide (indicated by red arrow). (See fig. 1*F*.)

Surface Faulting

Coseismic surface fault ruptures occurred throughout the affected area on at least 12 major transpressional faults as well as on several minor faults (Hamling and others, 2017; Stirling and others, 2017). GNS Science and partners have been conducting detailed surveys to measure displacements across surface fault ruptures (Litchfield and others, 2017). Dextral slip as great as 12 m and vertical offsets as great as 7 m along the Kekerengu and Papatea faults, respectively, northeast of Kaikoura (see fig. 3) have been documented (Hamling and others, 2017). Elsewhere, displacements generally range from 0.1 to 2 m. Documenting surface faulting was not our primary objective, but it was found to be relevant to landsliding because many of the large, deep landslides occur directly on or very close to surface fault displacements (fig. 17). The role played by the surface fault displacement in triggering these landslides requires further investigation.

We also encountered surface fault offsets throughout the study area unrelated to landsliding; such features were visible both on the ground and from the air, clearly offsetting roads, railways, and river channels (figs. 18–20). In some locations, differentiating surface fault offsets from cracking due to ground failure and ground shaking was difficult (fig. 21).

Figure 18. Photograph showing the Papatea fault offsetting State Highway 1 and South Island Main Trunk rail line near Waipapa Bay, aerial view. (See fig. 1*F*.)

Figure 19. Photograph showing the Papatea fault offsetting State Highway 1 and South Island Main Trunk rail line near Waipapa Bay, ground view. (See fig. 1*F*.)

Figure 20. Photograph showing the Kekerengu fault extending through alluvium in the Clarence River channel. (See fig. 1*E*.)

Figure 21. Photograph showing ground cracks along the trace of the Kekerengu fault about 10 kilometers northwest of Waipapa Bay. (See fig. 1*D*.)

Effects on People and Infrastructure

Considering the magnitude of the earthquake, effects on people and infrastructure were relatively limited because the strongest ground shaking was concentrated in a sparsely populated area. Only two fatalities related to the earthquake were reported, one from a collapsed structure in Kaikoura and the other from a heart attack (U.S. Geological Survey, 2017b). Ground-shaking damage to structures (fig. 22) was limited and scattered because of the paucity of structures in the earthquake area, but many agricultural buildings were damaged.

As much as 11 m of surface faulting offset roads and rail lines in several areas along the coast and in the Seaward Kaikoura Range. Dramatic examples of this occurred along SH1 near Waipapa Bay, where several meters of vertical and horizontal fault offset on the Papatea fault displaced the road and adjacent rail line (see figs. 18 and 19). A house was destroyed by surface rupture on the Kekerengu fault (fig. 23).

Figure 22. Photographs of ground-shaking damage to structures. *A*, Damaged exterior walls at Ward Fire Station. (See fig. 1*E*.) *B*, Stone tower toppled from Saint Oswald's Church about 13 kilometers south of Ward along State Highway 1. (See fig. 1*E*.)

Figure 23. Photograph showing a house damaged by displacement on the Kekerengu fault about 20 kilometers north-northeast of Waipapa Bay. (See fig. 1*E*.)

Figure 24. Photograph showing railroad tracks disrupted by ground deformation 16 kilometers southwest of Ward. (See fig. 1*E*.)

Even in areas not directly affected by surface fault offset, rail lines were displaced and rendered unusable by the effects of strong ground shaking, fill settlement, and crustal deformation (folding and subsidence) (fig. 24). Several river bridges were damaged or destroyed by strong ground shaking and fault offset (fig. 25).

Landslides triggered by the earthquake caused a great deal of damage to regional transportation systems. SH1, the principal road connecting Picton and Blenheim (on the north end of the South Island) to Christchurch (on the central east coast) was blocked in numerous places by both small and large landslides (figs. 26 and 27). Some of the largest landslides are likely to take months to stabilize and clear, and the coastal section of SH1 remained closed in July 2017 and might need to be fundamentally reengineered in some areas (see fig. 6). Tunnel portals were blocked by landslide debris in some areas (fig. 28). The SIMT rail line parallels SH1 along the coast and was similarly disrupted by landslides (fig. 29). Landslides also severely

Figure 27. Photograph showing State Highway 1 and the South Island Main Trunk rail line blocked by landslides about 7 kilometers southwest of Waipapa Bay. (See fig. 1*F*.)

Figure 25. Photograph showing a destroyed bridge over the Clarence River. (See fig. 1*D*.)

Figure 28. Photograph showing a landslide blocking State Highway 1 and a tunnel portal west of Kaikoura. (See fig. 1*B*.)

Figure 26. Photograph showing landslides blocking State Highway 1 between Waipapa Bay and Kaikoura. (See fig. 1*B*.)

Figure 29. Photograph showing the South Island Main Trunk rail line along State Highway 1 blocked by landslides about 7 kilometers southwest of Waipapa Bay. (See fig. 1*F*.)

Figure 30. Photograph showing a landslide blocking a minor road along the Clarence River. (See fig. 1*D*.)

disrupted secondary roads and local farm roads in the interior part of the island (fig. 30).

Valley-blocking landslides that dam rivers and streams are a major post-earthquake hazard. After this earthquake, they altered stream drainages, inundated upstream areas with impounded water, and damaged roads and trails. Some of these landslide dams breached safely and are passing water in a controlled fashion with little residual upstream impoundment. Others are likely to remain until tested by more significant rain or snowmelt events. Some could persist for the foreseeable future and form semipermanent lakes and ponds.

Crustal deformation from the fault movement uplifted large areas of the previously submerged coastal platform to above sea level (fig. 31; also see fig. 17). Other areas along the coast subsided and were inundated with water following the earthquake (fig. 32). This deformation affected roads and rail lines (fig. 33) and disrupted stream drainages; the widespread subsidence could result in continued flooding problems in the Kaikoura region.

Comparison of Observed and Modeled Landslide Distribution

We have been working with collaborators to develop a suite of coseismic landslide and liquefaction models that will provide near-real-time estimates of coseismic ground-failure hazards based on USGS ShakeMap ground-shaking estimates and other globally and regionally available input layers (Allstadt and others, 2016). An objective of our field reconnaissance was to (1) qualitatively assess how well the models performed for the Kaikoura earthquake, (2) identify possible sources of error, and (3) determine how the models can be improved. Our focus is on the coarser resolution global landslide models (approx. 1-km grid cells); these include Nowicki and others (2014), which estimates the probability of any landslide occurring in a given grid cell, and Godt and others (2008), which estimates the percentage of a given cell that could be affected by landsliding. Both models require ShakeMap PGA estimates, so we ran the models using ShakeMap version 7 (fig. 34*A*), the most up-to-date version available at the time we were in the field. Figure 3 shows the most recent version (ShakeMap version 16), which has been updated with better constrained faults and more strong-motion data.

Figure 31. Photograph showing uplifted marine platforms about 10 kilometers southwest of Waipapa Bay. (See fig. 1*B*.)

Figure 32. Photograph showing ponding in a subsided area astride the Kekerengu fault (indicated by white arrows) 15 kilometers southwest of Ward. (See fig. 1*E*.)

Figure 33. Photograph showing the South Island Main Trunk rail line offset laterally and vertically by the Kekerengu fault 15 kilometers southwest of Ward. (See fig. 1*E*.)

A quantitative assessment of modeled landslide probabilities will not be possible until a detailed landslide inventory is published, but our qualitative assessment indicates that both models overpredict landsliding. Both models correctly identify areas that were affected by landsliding, but they overpredict the extent of landsliding in those areas and do not correctly characterize areas not strongly affected by landslides (fig. 34*B*–*C*). For example, both models show high probabilities where landsliding was densest, including within the Seaward Kaikoura Range; in the lower relief areas affected by large, deep landslides northeast of Waiau; and along the coastal cliffs that produced landslides that blocked SH1 both north and south of Kaikoura (see fig. 34*B*–*C*). However, both models greatly overestimated landslide probabilities outside of these areas of dense landsliding, such as in the Inland Kaikoura Range. One reason for the poor model predictions in this area is that ground-shaking estimates in the Inland Kaikoura Range in ShakeMap version 7 were too high; this version included the Awatere fault (northwesternmost fault in fig. 3), which was later determined not to have slipped in this event. This misfit between model prediction and observation

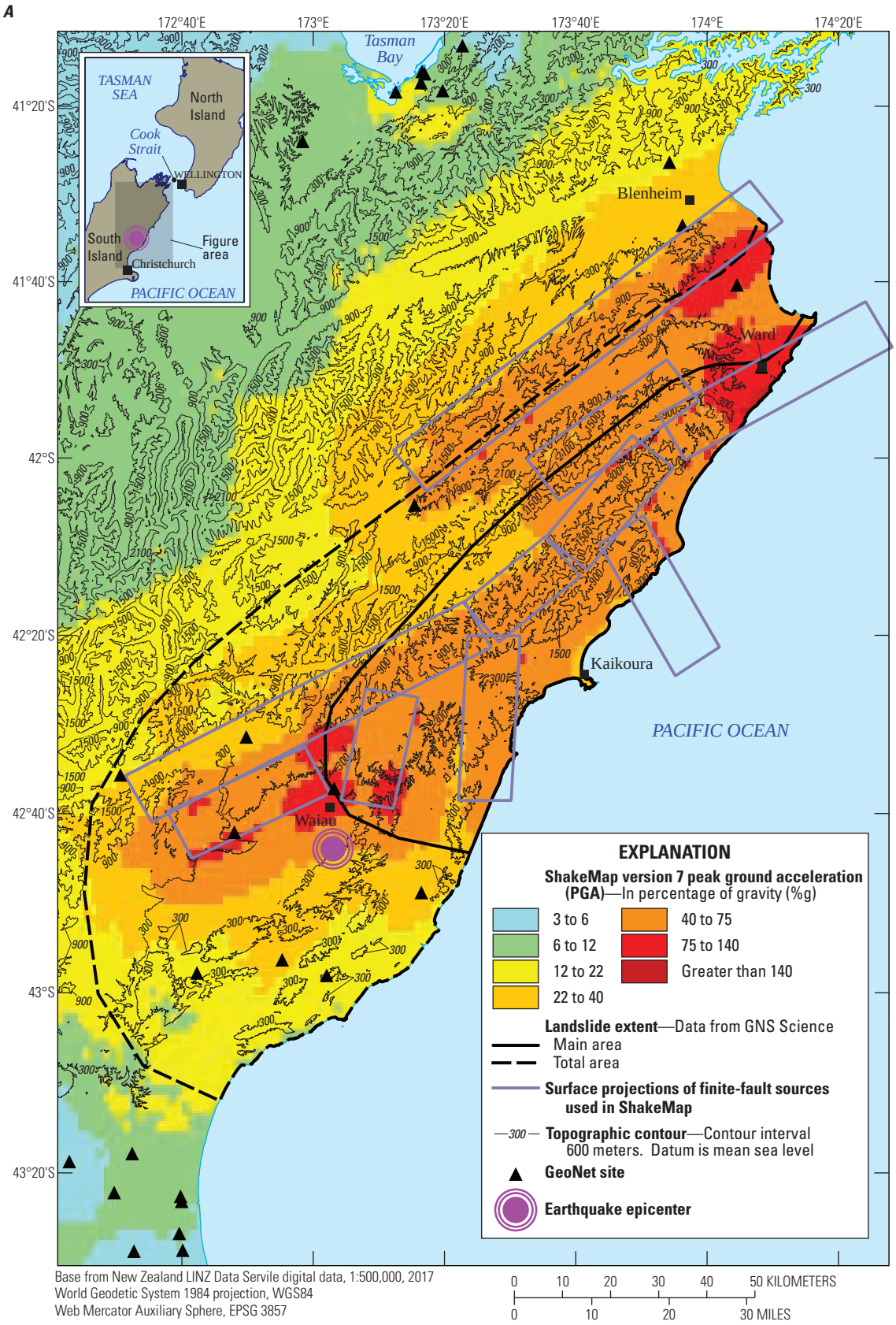

Figure 34. Maps showing ground shaking and predicted landslide probabilities for the 2016 Kaikoura, New Zealand, earthquake (approx. 1-kilometer resolution). *A*, Peak ground acceleration estimates made using U.S. Geological Survey ShakeMap version 7 (available on November 19, 2016, five days after the earthquake).

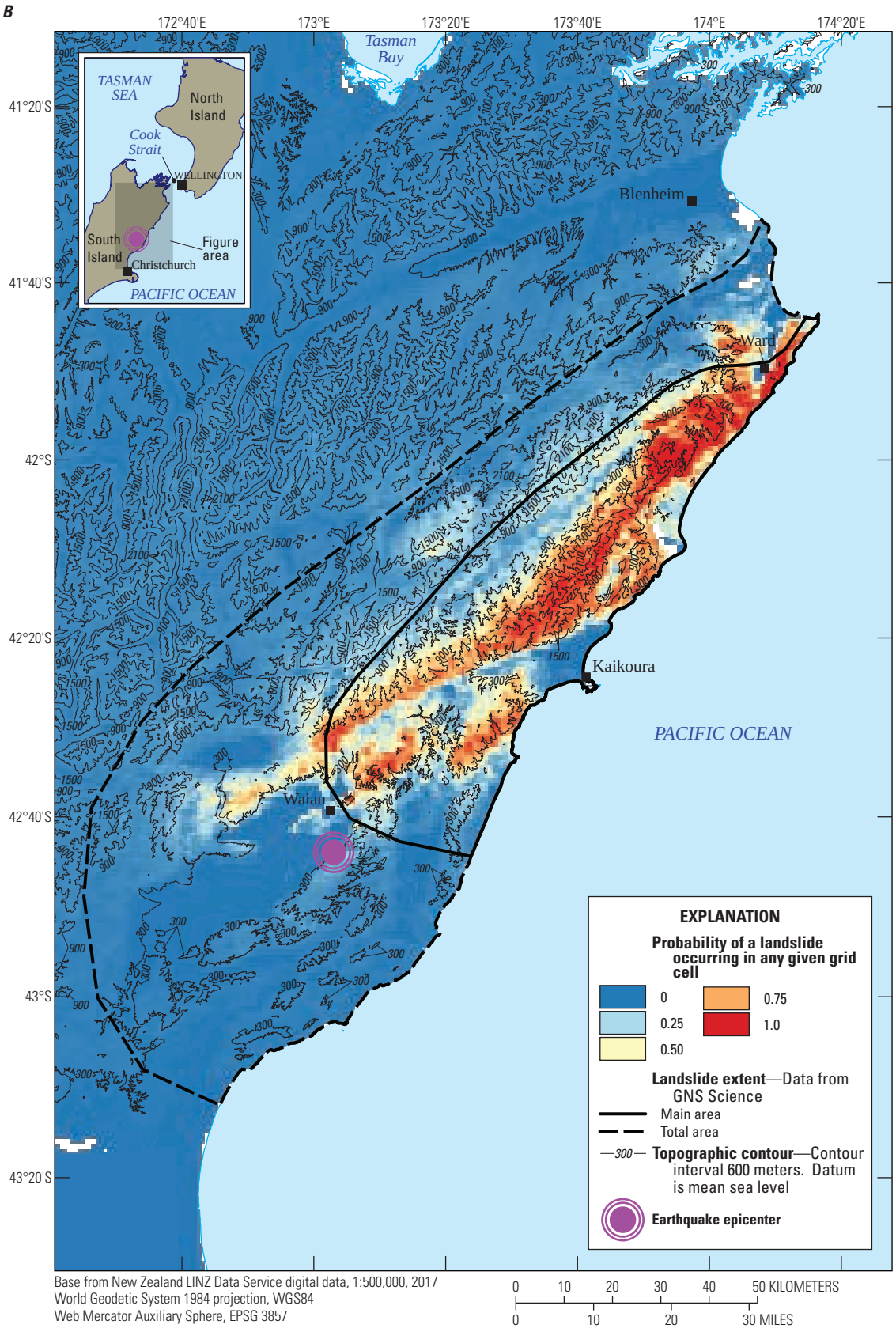

Figure 34. Maps showing ground shaking and predicted landslide probabilities for the 2016 Kaikoura, New Zealand, earthquake (approx. 1-kilometer resolution). *B*, Probability of a landslide occurring in a given grid cell, based on the model by Nowicki and others (2014).—Continued

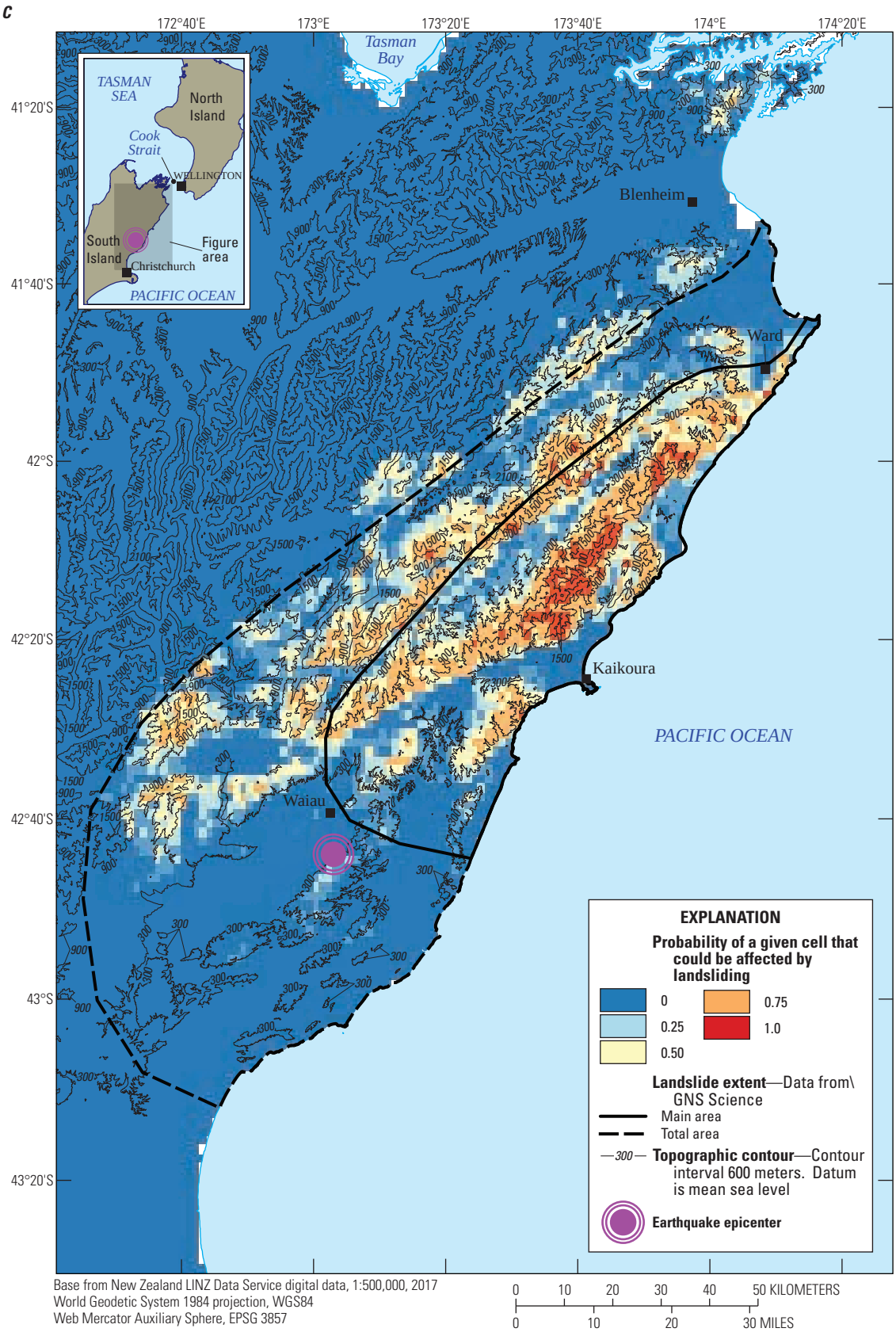

Figure 34. Maps showing ground shaking and predicted landslide probabilities for the 2016 Kaikoura, New Zealand, earthquake (approx. 1-kilometer resolution). *C*, Percentage of a given grid cell that could be affected by landsliding, based on the model by Godt and others (2008).—Continued

demonstrates that, in near real time, incomplete or inaccurate input data can strongly skew the estimated ground-shaking and ground-failure hazard estimates; thus, a way of accounting for and communicating uncertainty is needed. ShakeMap estimates some sources of ground-shaking uncertainties, but currently it does not account for epistemic uncertainties that can arise from errors such as a nonseismogenic fault. Likewise, the ground-failure models do not account for uncertainties in their input parameters (such as rock strength), which can be significant (Dreyfus and others, 2013).

An area of overestimation that is less easily explained is the area around Ward, where both ground-failure models estimate high landslide probabilities but where we found few slope failures. Recorded ground shaking at Ward exceeded 1 g, and the ShakeMap algorithm assumes that if shaking is high at a strong-motion station, it is also high for a certain radius around that station after adjusting for differing site conditions (Worden and others, 2010). Figure 34*A* shows a patch of high PGA around Ward that extends into the surrounding hills, which, in turn, generated high landslide probability estimates there; landslides in that area were not confirmed by observations. Although we cannot currently explain this discrepancy, possible explanations include the following: (1) the high PGA recorded at Ward is a highly localized anomaly attributable to site amplification; (2) although the PGA was high, other ground-motion parameters such as frequency and duration were not conducive to landslide triggering; or (3) geologic conditions in nearby sloping areas were mischaracterized in the models. Though high ground accelerations can significantly decrease effective stress on a shear surface and increase downslope driving forces on a potential landslide mass, the frequency and duration of the ground motion also are important (Jibson and others, 2004; Jibson, 2011). Transient spikes of high-frequency PGA commonly generate little slope displacement (Newmark, 1965) and thus contribute little to slope-failure probability. Other ground-motion parameters might be more effective at estimating landslide probabilities. For example, Jibson (2007) developed a model relating estimated landslide displacement (and thus failure probability) to Arias (1970) intensity, which implicitly accounts for frequency and duration in addition to the amplitude of acceleration. Also, a newer revision of the Nowicki and others (2014) model uses PGV rather than PGA; PGV is less sensitive to isolated peaks and does not saturate with magnitude, and this model does not estimate high landslide probabilities around Ward (M.A. Jessee, Indiana University Bloomington, oral commun., 2017). These options for ground-motion parameterization provide opportunities for future model development.

Summary and Conclusions

The 2016 Kaikoura, New Zealand, earthquake triggered widespread landslides that dammed rivers and blocked roads and rail lines. Observations from our reconnaissance of the area after the earthquake include the following salient points:

- Thousands of landslides were triggered over an area of at least 12,000 square kilometers in the northeastern part of the South Island. Landslides primarily were concentrated in the Seaward Kaikoura Range and surrounding areas of lower topography.
- Most of the landslides occurred in Lower Cretaceous graywacke sandstone that predominates in this area. Landslides in this material generally were highly disrupted falls and slides, some of which transformed into debris avalanches that blocked valleys and dammed rivers.
- Weak Upper Cretaceous to Neogene sedimentary rock that surrounds the graywacke produced deeper, more coherent slumps and block slides. Many of these deeper landslides also blocked rivers and created substantial hazards from potential breach of impounded lakes. The likelihood and results of breach were not analyzed as part of this work.
- Many of the largest landslides clustered along faults that produced surface displacement, which suggests a possible causative relationship.
- We used observations from this earthquake to qualitatively evaluate two models that predict landslide probabilities in near real time following earthquakes. Both models we examined did well at predicting areas where landslides were observed but significantly overpredicted landslide probabilities in areas where we observed few or no landslides.

Observations in this report are preliminary. GNS Science is leading research efforts in more detailed and quantitative studies in collaboration. The appendix contains more detailed observations and photographs of the areas investigated.

References Cited

Allstadt, K.E., Thompson, E.M., Wald, D.J., Hamburger, M.W., Godt, J.W., Knudsen, K.L., Jibson, R.W., Jessee, M.A., Zhu, Jing, Hearne, Michael, Baise, L.G., Tanyas, Hakan, and Marano, K.D., 2016, USGS approach to real-time estimation of earthquake-triggered ground failure—Results of 2015 workshop: U.S. Geological Survey Open-File Report 2016–1044, 13 p.

Arias, Arturo, 1970, A measure of earthquake intensity, *in* Hansen, R.J., ed., Seismic design for nuclear power plants: Cambridge, Massachusetts Institute of Technology Press, p. 438–483.

Ashford, S.A.; Sitar, Nicolas; Lysmer, John; and Deng, Nan, 1997, Topographic effects on the seismic response of steep slopes: Seismological Society of America Bulletin, v. 87, no. 3, p. 701–709.

Collins, B.D., and Jibson, R.W., 2015, Assessment of existing and potential landslide hazards resulting from the April 25, 2015 Gorkha, Nepal earthquake sequence: U.S. Geological Survey Open-File Report 2015–1142, 50 p.

Dellow, Sally; Massey, Chris; Cox, Simon; Archibald, Garth; Begg, John; Bruce, Zane; Carey, Jon; Davidson, Jonathan; Della Pasqua, Fernando; Glassey, Phil; Hill, Matt; Jones, Katie; Lyndsell, Barbara; Lukovic, Biljana; McColl, Sam; Rattenbury, Mark; Read, Stuart; Rosser, Brenda; Singeisen, Corinne; Townsend, Dougal; Villamor, Pilar; Villeneuve, Marlene; Wartman, Joseph; Rathje, Ellen; Sitar, Nick; Adda, A.Z.; Manousakis, John; and Little, Michael, 2017, Landslides caused by the Mw7.8 Kaikiōura earthquake and the immediate response: Bulletin of the New Zealand Society for Earthquake Engineering, v. 50, no. 2, p. 106–116.

DigitalGlobe, 2016, EV WebHosting image database: DigitalGlobe, accessed November 30, 2016, at https://evwhs.digitalglobe.com/.

Dreyfus, Daniel, Rathje, E.M., and Jibson, R.W., 2013, The influence of different simplified sliding-block models and input parameters on regional predictions of seismic landslides triggered by the Northridge earthquake: Engineering Geology, v. 163, p. 41–54.

Environment Canterbury, 2017, North Canterbury landslide dams—Following the 7.8 magnitude earthquake on the 14th November 2016: Environment Canterbury [New Zealand] web page, accessed April 28, 2017, at http://ecan.maps.arcgis.com/apps/Cascade/index.html?appid=50f00d42e29c46b1a61b848440c5295a.

GeoNet, 2016a, How is the Kaikoura aftershock sequence behaving compared to the forecast?: GeoNet web page, accessed February 12, 2017, at http://info.geonet.org.nz/pages/viewpage.action?pageId=20545914.

GeoNet, 2016b, Landslides, dams, and a reminder to take care in the outdoors over the holidays: GeoNet web page, accessed October 4, 2017, at http://www.geonet.org.nz/news/6c9MonfWj60EEGUIwCQwQy.

Geotechnical Extreme Events Reconnaissance, 2017, 2016 Kaikoura, New Zealand earthquake: Geotechnical Extreme Events Reconnaissance web page, accessed March 3, 2017, at https://doi.org/10.18118/G6NK57.

Godt, J.W., Şener, Başak, Verdin, K.L., Wald, D.J., Earle, P.S., Harp, E.L., and Jibson, R.W., 2008, Rapid assessment of earthquake-induced landsliding, *in* World Landslides Forum, 1st, Tokyo, November 18–21, 2008, Proceedings: Tokyo, United Nations University, p. 219–222.

Hamling, I.J.; Hreinsdóttir, Sigrun; Clark, Kate; Elliott, John; Liang, Cunren; Fielding, Eric; Litchfield, Nicola; Villamor, Pilar; Wallace, Laura; Wright, T.J.; D'Anastasio, Elisabetta; Bannister, Stephen; Burbidge, David; Denys, Paul; Gentle, Paula; Howarth, Jamie; Mueller, Christof; Palmer, Neville; Pearson, Chris; Power, William; Barnes, Philip; Barrell, D.J.A.; Van Dissen, Russ; Langridge, Robert; Little, Tim; Nicol, Andrew; Pettinga, Jarg; Rowland, Julie; and Stirling, Mark, 2017, Complex multifault rupture during the 2016 M_w 7.8 Kaikōura earthquake, New Zealand: Science, first release posted March 23, 2017, 16 p., accessed April 3, 2017, at https://doi.org/10.1126/science.aam7194.

Jibson, R.W., 2007, Regression models for estimating coseismic landslide displacement: Engineering Geology, v. 91, p. 209–218.

Jibson, R.W., 2011, Methods for assessing the stability of slopes during earthquakes—A retrospective: Engineering Geology, v. 122, p. 43–50.

Jibson, R.W., Harp, E.L., Schulz, William, and Keefer, D.K., 2004, Landslides triggered by the 2002 Denali fault, Alaska, earthquake and the inferred nature of the strong shaking: Earthquake Spectra, v. 20, p. 669–691.

Keefer, D.K., 1984, Landslides caused by earthquakes: Geological Society of America Bulletin, v. 95, no. 4, p. 406–421.

Keefer, D.K., 2002, Investigating landslides caused by earthquakes—A historical review: Surveys in Geophysics, v. 23, no. 6, p. 473–510.

Keefer, D.K., and Manson, M.W., 1998, Regional distribution and characteristics of landslides generated by the earthquake, *in* Keefer, D.K., ed., The Loma Prieta, California, earthquake of October 17, 1989—Landslides: U.S. Geological Survey Professional Paper 1551–C, p. C7–C32.

Litchfield, N.J., Benson, A., Bischoff, A., Hatem, A., Barrier, A., Nicol, A., Wandres, A., Lukovic, B., Hall, B., Gasston, C., Asher, C., Grimshaw, C., Madugo, C., Fenton, C., Hale, D., Barrell, D.J.A., Heron, D.W., Strong, D.T., Townsend, D.B., Nobe, D., Howarth, J.D., Pettinga, J., Kearse, J., Williams, J., Manousakis, J., Mountjoy, J., Rowland, J., Clark, K.J., Pedley, K., Sauer, K., Berryman, K.R., Hemphill-Haley, M., Stirling, M.W., Villeneuve, M., Cockroft, M., Khajavi, N., Barnes, P., Villamor, P., Carne, R., Langridge, R.M., Zinke, R., Van Dissen, R.J., McColl, S., Cox, S.C., Lawson, S., Little, T., Stahl, T., Cochran, U.A., Toy, V., Ries, W.F., and Juniper, Z., 2017, 14th November 2016 M7.8 Kaikoura earthquake—Summary surface fault rupture traces and displacement measurements: GNS Science image, accessed March 4, 2017, at https://doi.org/10.21420/G2RC7C.

Malamud, B.D., Turcotte, D.L., Guzzetti, Fausto, and Reichenbach, Paola, 2004, Landslide inventories and their statistical properties: Earth Surface Processes and Landforms, v. 29, no. 6, p. 687–711.

Massey, C.I., Townsend, D.B., Rosser, B.J., Villeneuve, M., McColl, S., Davidson, J., Carey, J.M., Lyndsell, B.M., Lukovic, B., Singeisen, C., Dellow, G.D., Cox, S.C., and Jones, K.E., 2017, Locations of landslides generated by the Kaikoura 2016 earthquake, version 1: GNS Science image, accessed April 5, 2017, at https://vml.gns.cri.nz/asset-bank/action/viewAsset?id=187586&index=1&total=4&view=viewSearchItem.

New Zealand Treasury, 2016, Economic and fiscal impacts of the Kaikōura earthquakes, *in* Half year economic and fiscal update: New Zealand Treasury, accessed January 30, 2017, at http://www.treasury.govt.nz/budget/forecasts/hyefu2016/007.htm.

Newmark, N.M., 1965, Effects of earthquakes on dams and embankments: Geotechnique, v. 15, p. 139–159.

Newshub, 2016, Cows stranded on “island” after New Zealand earthquake—Aerial video: The Guardian video, 0:21 min, posted November 14, 2016, accessed January 25, 2017, at https://www.theguardian.com/world/video/2016/nov/14/cows-stranded-on-island-after-new-zealand-earthquake-aerial-video.

Nowicki, M.A., Wald, D.J., Hamburger, M.W., Hearne, Michael, and Thompson, E.M., 2014, Development of a globally applicable model for near real-time prediction of seismically induced landslides: Engineering Geology, v. 173, p. 54–65.

Rathje, Ellen; Little, M.; Wartman, Joseph; Athanasopoulos-Zekkos, A.; Massey, Chris; and Sitar, Nicolas, in press, Preliminary landslide inventory for the 2016 Kaikoura, New Zealand earthquake derived from satellite imagery and aerial/field reconnaissance, version 1: Geotechnical Extreme Events Reconnaissance (GEER) Association.

Rathje, Ellen, Little, M., Massey, Chris, and Wartman, Joseph, 2017, Kaikoura earthquake landslide inventory: Design-Safe-CI, dataset, accessed October 20, 2017, at https://doi.org/10.17603/DS2508W.

Rattenbury, M.S., Townsend, D.B., and Johnston, M.R., comps., 2006, Geology of the Kaikoura area: GNS Science, Institute of Geological and Nuclear Sciences [New Zealand], Geological Map 13, 1 sheet, scale 1:250,000, 70-p. pamphlet.

Stirling, M.W., Litchfield, N.J., Villamor, P., Van Dissen, R.J., Nicol, A., Pettinga, J., Barnes, P., Langridge, R.M., Little, T., Barrell, D.J.A., Mountjoy, J.W., Ries, F., Rowland, J., Fenton, C., Hamling, I., Asher, C., Barrier, A., Benson, A., Bischoff, A., Borella, J., Carne, R., Cochran, U.A., Cockroft, M., Cox, S.C., Duke, G., Fenton, F., Gasston, C., Grimshaw, C., Hale, D., Hall, B., Hao, K.X., Hatem, A., Hemphill-Haley, M., Heron, D.W., Howarth, J., Juniper, Z., Kane, T., Kearse, J., Khajavi, N., Lamarche, G., Lawson, S., Lukovic, B., Madugo, C., Manousakis, J., McColl, S., Noble, D., Pedley, K., Sauer, K., Stahll, T., Strong, D.T., Townsend, D.B., Toy, V., Villeneuve, M., Wandres, A., Williams, J., Woelz, S., and Zinke, R., 2017, The M_w 7.8 2016 Kaikōura earthquake—Surface fault rupture and seismic hazard context: Bulletin of the New Zealand Society for Earthquake Engineering, v. 50, no. 2, p. 73–84.

U.S. Geological Survey, 2017a, M 7.8—54km NNE of Amberley, New Zealand—Finite fault: U.S. Geological Survey web page, accessed January 15, 2017, at http://earthquake.usgs.gov/earthquakes/eventpage/us1000778i#finite-fault.

U.S. Geological Survey, 2017b, M 7.8—54km NNE of Amberley, New Zealand—Impact: U.S. Geological Survey web page, accessed January 12, 2017, at https://earthquake.usgs.gov/earthquakes/eventpage/us1000778i#impact.

U.S. Geological Survey, 2017c, M 7.8—54km NNE of Amberley, New Zealand—Overview: U.S. Geological Survey web page, accessed January 15, 2017, at https://earthquake.usgs.gov/earthquakes/eventpage/us1000778i#executive.

U.S. Geological Survey, 2017d, ShakeMap: U.S. Geological Survey web page, accessed October 10, 2017, at https://earthquake.usgs.gov/data/shakemap/.

Valkaniotis, Sotiris; Papathanassiou, George; and Pavlides, Spyros, 2016, Preliminary map of co-seismic landslides for the M 7.8 Kaikoura, New Zealand earthquake [dataset]: Zenodo, accessed December 1, 2016, at https://doi.org/10.5281/zenodo.167130.

Varnes, D.J., 1978, Slope movement types and processes, *in* Schuster, R.L., and Krizek, R.J., eds., Landslides—Analysis and control: Washington, D.C., Transportation Research Board Special Report 176, p. 11–33.

Wald, D.J., Quitoriano, Vince, Heaton, T.H., Kanamori, Hiroo, Scrivner, C.W., and Worden, B.C., 1999, TriNet "ShakeMaps"—Rapid generation of peak ground motion and intensity maps for earthquakes in southern California: Earthquake Spectra, v. 15, p. 537–556.

Wald, D.J., Worden, B.C., Quitoriano, Vince, and Pankow, K.L., 2005, ShakeMap manual—Technical manual, user's guide, and software guide: U.S. Geological Survey Techniques and Methods, book 12, chap. A1, 128 p.

Worden, C.B., Wald, D.J., Allen, T.I., Lin, K., Garcia, D., and Cua, G., 2010, A revised ground-motion and intensity interpolation scheme for ShakeMap: Seismological Society of America Bulletin, v. 100, no. 6, p. 3083–3096.

Appendix. Field Reconnaissance Observations

This appendix provides a general overview of the landslides and other geologic effects we observed in three physiographically distinct regions of the area affected by the 2016 Kaikoura, New Zealand, earthquake (fig. 35):

- *Cape Campbell to Waipapa Bay.*—This area is a coastal margin composed of Quaternary low-lying beaches and uplifted marine terraces backed by hilly areas composed of Neogene to Upper Cretaceous sedimentary rock interspersed with Lower Cretaceous graywacke sandstone and argillite. Landslides included rock falls and debris avalanches in steeper terrain and slides and slumps in less steep areas. The Sea Front (Cow Slip) landslide, described below, is the largest landslide in this area (see fig. 17).
- *Waipapa Bay to Mount Lyford.*—This area includes the Seaward Kaikoura Range, where Lower Cretaceous graywacke sandstone forms high ridges and steep topography. The Clarence River, a long fluvial system controlled by northeast-trending regional faulting,

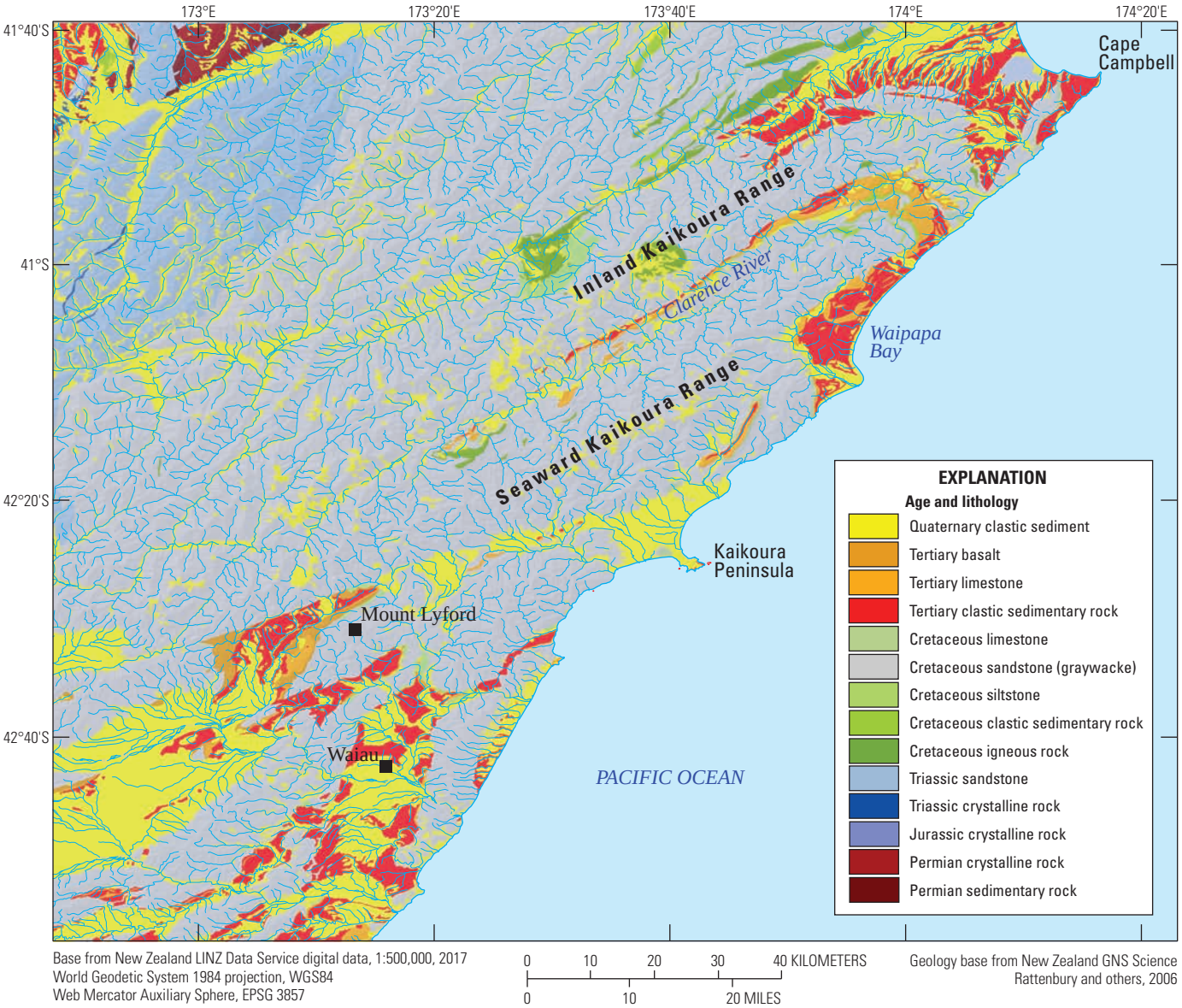

Figure 35. Geologic map of the 2016 Kaikoura, New Zealand, earthquake landslide reconnaissance area. (Modifed from Rattenbury and others, 2006.)

separates the Seaward and Inland Kaikoura Ranges; landslides were abundant in the Seaward Kaikoura Range but ended abruptly at the valley of the Clarence River. Resistant Paleogene limestone forms hard points in the landscape, most notably Sawcut Gorge, where slot canyons deeply incise the resistant limestone. (See also fig. 1*A*–*B*.)

- *Mount Lyford to Waiau.*—This area is characterized by rolling hills composed of weak Upper Cretaceous to Neogene sedimentary rock (both marine and nonmarine) that produced several deep coherent slides that blocked rivers and streams.

The locations of the landslides described in this appendix are shown in figure 1*A*. With few exceptions, we identify these landslides by using the naming convention developed by GNS Science (Institute of Geological and Nuclear Sciences Limited): the name of the drainage blocked by the landslide and the approximate elevation in meters above sea level. The Cape Campbell and Sea Front landslides do not block drainages and therefore do not have elevations as part of their names.

Cape Campbell to Waipapa Bay

At Cape Campbell, we observed a surface fault rupture on a previously unmapped fault that has been named the Lighthouse fault by GNS Science (fig. 36). Fault displacement averaged about 0.5 meter (m) of vertical displacement. Visible surface faulting extended approximately 1 kilometer (km) from the south-facing shoreline on the south end of Cape Campbell northward toward the tip of the cape.

A large preexisting landslide on a hill composed of weak Neogene sandstone and siltstone was reactivated and significantly enlarged by the earthquake shaking (fig. 37). Extensive ground cracking on the crest of the hill indicates incipient failure of larger parts of the hillside (fig. 38). Numerous other preexisting landslides on steep slopes in weak sediment in the vicinity of Cape Campbell were reactivated and enlarged by strong shaking (fig. 39).

From Blenheim to Ward, we observed numerous failures on steep, unengineered roadcuts and fill embankments (fig. 40). On the coast, just east of Ward, we saw several landslide scars, but many of them appeared to be preexisting features that might have been partially reactivated during the earthquake.

In the steeper Inland Kaikoura Range about 8 km west of Ward, we observed landslides that transitioned into steep debris flow-like channels (fig. 41). From a distance, we could not determine if these channels formed from rapid dry granular flow or if enough water was present to form a true debris flow.

Just south of Ward, we followed the Ure River up toward Sawcut Gorge. The Ure River is braided and choked with large boulders and cobbles; much of this sediment is landslide debris derived from the steep-walled canyons upstream. We saw fresh landslides, presumably from the most recent earthquake, within the fluvial corridor that directly supplied sediment to the river. Some of these slides occurred on the ends of ridges (fig. 42). They are commonly called “nose” or “spur-end” failures and are common in earthquakes, most likely because of topographic amplification (Keefer and Manson, 1998).

Figure 36. Photograph showing surface fault rupture on Cape Campbell. (See fig. 1*C*.)

Upstream, the river narrows into Sawcut Gorge, a resistant limestone block that has been narrowly incised. Landslides in this steep terrain created multiple in-channel dams that formed chains of ponds in the gorge (see fig. 9).

About 13 km south of Ward along State Highway 1, we saw structural damage to St. Oswald’s Church (see fig. 22*B*).

Figure 37. Photograph showing a preexisting landslide on Cape Campbell that was reactivated and significantly enlarged during the earthquake. (See fig. 1*C*.)

Figure 38. Photograph showing a fresh crack on crest of hillside above Cape Campbell landslide. (See figs. 1*C* and 37.)

Figure 40. Photograph showing landslides from roadcuts between Blenheim and Ward. (See fig. 1*E*.)

Figure 39. Photograph showing reactivated landslides on coastal bluffs west of Cape Campbell. (See fig. 1*C*.)

Figure 41. Photograph showing debris slides about 8 kilometers west of Ward. (See fig. 1*E*.)

Figure 42. Photograph showing fresh landslide on the end of a ridge directly entering the Ure River near Sawcut Gorge. (See fig. 1*E*.)

A few kilometers farther south, State Highway 1 was damaged from surface fault rupture, and a down-dropped block adjacent to the coast created a temporary lake (see fig. 32). Because the new lake is not connected to the ocean, it presumably is filled by groundwater seepage and surface drainage. This location also experienced significant damage to the railway (see fig. 33).

The Clarence River discharges into the ocean at Waipapa Bay. At about 20 km upstream from its mouth, looking downstream, the river turns abruptly to the southeast and cuts through the Seaward Kaikoura Range. Just north of this sharp turn, we saw several steep landslides with substantial cracks uphill of the landslide main scarp (fig. 43). Farther north in the Seaward Kaikoura Range, we saw additional landsliding that transitioned into debris slides with flow-like features (fig. 44).

Perhaps the most widely reported landslide caused by the earthquake is the Sea Front landslide, originally referred to as the Cow Slip landslide because of a widely viewed aerial video (Newshub, 2016) showing several cows stranded on an isolated

Figure 43. Photograph showing hillside cracks that indicate incipient landslide movement above the shallow failure triggered by the earthquake in the Seaward Kaikoura Range. (See fig. 1*E*.)

Figure 44. Photograph showing debris slides triggered by the earthquake in the Seaward Kaikoura Range. (See fig. 1*E*.)

landslide block. This landslide is a complex feature involving slumping, sliding, toppling, and disaggregated flow of late Miocene calcareous silty mudstone of the Waima Formation (fig. 45). The landslide has an estimated volume of 6,000,000 cubic meters (m^3) and a total length of about 1,100 m (Massey and others, 2017). The Papatea fault, which produced surface rupture during the earthquake, comes onshore just south of the Sea Front landslide, passes through the landslide source area, and continues along smaller ridges to the north that also produced smaller landslides during the earthquake. The upper parts of the slide moved as coherent—though extensively fractured—blocks (fig. 46). The central part of the slide is chaotic, with evidence of backward, lateral, and forward rotation of distinct landslide blocks (fig. 47). The toe of the landslide transformed into disaggregated earth flows that moved into two drainages (fig. 48).

Figure 45. Photograph showing the Sea Front landslide near Waipapa Bay. (See fig. 1*D*.)

Figure 47. Photograph showing the central part of the Sea Front landslide. (See fig. 1*D*.)

Figure 46. Photograph showing the main scarp and upper part of the Sea Front landslide. (See fig. 1*D*.)

Figure 48. Photograph showing the toe of the Sea Front landslide that transformed into an earth flow. (See fig. 1*D*.)

Waipapa Bay to Mount Lyford (Seaward Kaikoura Range)

The greatest concentration of landslides triggered by the earthquake is in the Seaward Kaikoura Range, an area of steep topography and peaks reaching an elevation of 2,600 m. The main backbone of this mountain range consists of Lower Cretaceous graywacke sandstone; both the northwestern and southeastern fringes of the range have outcrops of Upper Cretaceous to Neogene marine and nonmarine sedimentary rock. Landslides in the graywacke generally are highly disrupted falls and slides in rock and debris (see figs. 6 and 7). Sizes range from a few tens of cubic meters to hundreds of thousands of cubic meters. The Upper Cretaceous to Neogene sedimentary rock produced several deep, coherent block slides and slumps that blocked valleys and dammed rivers (see fig. 8). Pervasive ground cracking in these rock units suggests incipient landsliding on many slopes as well as failure caused by lurching during the strong ground shaking (see figs. 12–14).

This section describes some of the larger and more significant landslides in the Seaward Kaikoura Range. Each of these landslides dammed a river valley and thus was a focus of concern following the earthquake.

Hapuku 740 Landslide

The Hapuku 740 landslide is a rock avalanche that occurred in the upper Hapuku River valley (fig. 49). With an estimated volume of more than 12,000,000 m^3, a source area of more than 650,000 square meters (m^2), and a length of 2,100 m, this was the largest landslide triggered by the earthquake (Massey and others, 2017). The slide occurred in basement graywacke and consists of coarse fractured blocks ranging in size from a few centimeters to several decimeters; scattered large (>1 m in diameter) boulders also are abundant. The landslide deposit contains a fine matrix of pulverized rock that renders the dam mostly impermeable and thus able to impound a lake approximately 350 m long by 100 m wide.

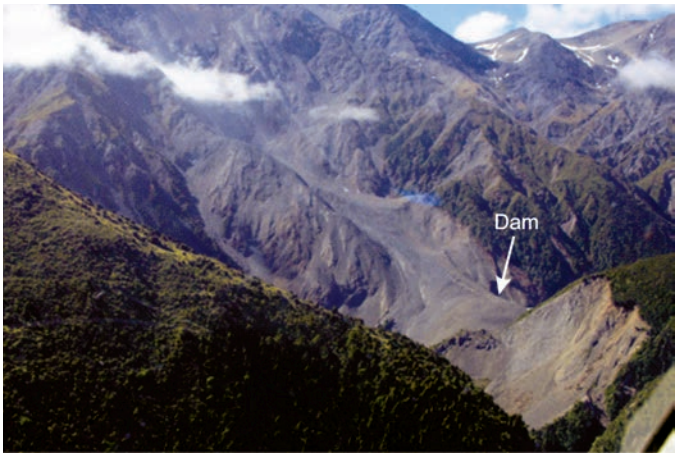

Figure 49. Photograph showing the Hapuku 740 rock avalanche and dam. (See fig. 1*B*.)

At the time of our visit, several seepage points and areas of headward erosion immediately behind the seepage points had formed on the downstream face of the dam (fig. 50), which presented a significant hazard that could cause the dam to fail catastrophically from some combination of headward erosion, internal erosion (piping), or overtopping of the impounded lake. The landslide source area consists of fairly planar surfaces that appear to be preexisting discontinuities in the rock mass. The trace of the Upper Kowhai fault extends through the landslide source area and probably influenced the location and geometry of the slide.

In April 2017, subsequent to our visit, Cyclone Cook produced heavy rainfall in the Hapuku drainage. Following this event, the dam partially failed by headward erosion above the seeps and was overtopped by the rising lake level; the result was a debris flood extending 3–4 km downstream (Chris Massey, GNS Science, written commun., 2017). Continuing seepage and erosion from the downstream face indicates that future heavy rainfall could cause additional erosion and overtopping episodes that would pose downstream risks.

Linton 340 Landslide

The Linton 340 landslide occurred in Lower Cretaceous graywacke that, in this area, is deeply weathered and soil-like in texture. The landslide, located astride the Kowhai fault but south of where Litchfield and others (2017) mapped surface

Figure 50. Photograph showing the downstream face of the Hapuku 740 landslide dam. Arrows indicate locations of seeps. (See fig. 1*B*.)

fault displacements, moved by a combination of slumping and sliding. The landslide blocked the Linton River, and the toe area appeared to have deformed through plastic flow (fig. 51). The landslide has a volume of about 1,000,000 m^3, a source area covering 95,000 m^2, and a length of 650 m (Massey and others, 2017). The Linton 340 slide pinched closed the river channel and impounded a lake of moderate size. In April 2017, rainfall from Cyclone Debbie overtopped the dam and caused a significant downstream flood that deposited debris for about 2 km downstream (Chris Massey, GNS Science, written commun., 2017).

Conway 420 Landslide

The Conway 420 landslide occurred in graywacke and blocked the Conway River just north of the Hope fault (fig. 52). Surface fault offsets were not mapped on the Hope fault in this area (Litchfield and others, 2017), and Hamling and others (2017) modeled negligible slip at depth here. The landslide has a volume of 500,000 m^3, a source area covering more than 50,000 m^2, and a length of 825 m (Massey and others, 2017). The landslide initiated as a highly disrupted rock slide from a planar failure surface that was likely a preexisting discontinuity in the rock mass (fig. 53); the geometry and run-up characteristics of the deposit indicate that the slide became a rock avalanche as velocity increased downslope. The deposit consists of fractured rock fragments and a fine-grained matrix of pulverized rock. The deposit formed a large, dome-shaped dam that impounded a lake 650 m long by about 100 m wide. At the time of our visit, it appeared from high-water marks that the lake had decreased in elevation 2–3 m from its peak sometime after the earthquake (fig. 54). The dam appeared stable at the time of our visit, but it was entirely washed away in April 2017 during heavy rainfall from cyclones (Chris Massey, GNS Science, written commun., 2017).

Figure 51. Photograph showing the Linton 340 landslide dam. (See fig. 1*B*.)

Figure 53. Photograph showing the planar failure surface of the Conway 420 landslide. (See fig. 1*G*.)

Figure 52. Photograph showing the Conway 420 landslide dam. (See fig. 1*G*.)

Figure 54. Photograph showing the lake impounded by the Conway 420 landslide dam. (See fig. 1*G*.)

Towy 500 Landslide

The Towy 500 landslide occurred in deeply weathered graywacke sandstone just north of the Hope fault (fig. 55). The landslide consists of a rock slide having a volume of about 500,000 m^3, a source area covering 62,000 m^2, and a length of 465 m (Massey and others, 2017). The landslide briefly blocked the Towy River, but at the time of our visit, the dam had largely breached (fig. 56), and the impounded lake upstream was considerably lower than its peak elevation (see fig. 55). Redeposited landslide material downstream from the breached dam caused aggradation of a few meters. Evidence including channel incision, debris lines, and disturbed vegetation indicates a maximum flood height of perhaps 2–4 m immediately downstream from the dam (fig. 57). Redeposition of dam material extended a few kilometers downstream.

Figure 55. Photograph showing the Towy 500 landslide dam and the remaining impounded lake. (See fig. 1*G*.)

Mount Lyford to Waiau

The lower elevation area between the coast and the Seaward Kaikoura Range west and south of Kaikoura (fig. 1), characterized by peak elevations of 300–960 m, was heavily affected by landsliding and landslide dams. In contrast to the shallower, disrupted landslides that dominate in the more rugged graywacke-dominated Seaward Kaikoura Range, this area experienced deeper, coherent landsliding in Neogene sedimentary rock, similar in style to the Sea Front landslide. Several fault zones extend through this area, and many of the larger landslides occurred on or near fault traces; thus, it appears that surface faulting was a contributing factor to the observed landslide style and distribution. The following sections describe some of the significant landslides in this area.

Leader 220 Landslide

The Leader River was dammed in more than a dozen places within two tributaries. The largest and potentially most hazardous of these is the Leader 220 landslide (figs. 58 and 59), with an estimated volume of 2,000,000 m^3, a source area covering almost 200,000 m^2, and length of about 1,100 m (Massey

Figure 56. Photograph showing the area where the Towy 500 landslide dam breached. (See fig. 1*G*.)

and others, 2017). This landslide occurred in the Neogene Greta Formation, which consists of marine siltstone, mudstone, sandstone, and limestone. At the time of our visit, the landslide abutted the terraces on the opposite side of the stream, and it entirely blocked the river and impounded a lake about 1 km long (fig. 60). At that time, water was flowing over the dam and was actively downcutting the dam, which suggested the possibility of rapid failure. As of February 22, 2017, the main dam had eroded, and water was flowing through the breach (Environment Canterbury, 2017). The North and South Leader fault zones extend through this area, but we cannot confirm that surface fault slip occurred directly below the landslide source area on these faults. Investigations subsequent to our visit confirm that a fault rupture along the Humps fault zone extends through the toe of the landslide debris (Chris Massey, GNS Science, written commun., 2017). This landslide is largely coherent, with intact and nearly upright forest on the upper half of the deposits. The toe is more disrupted but has patches of tilted vegetation still clumped together.

Figure 57. Photograph showing deposits of the eroded Towy 500 landslide dam burying trees near original river channel. (See fig. 1*G*.)

Stanton 200 Landslide

Just over the drainage divide southeast of the Leader 220 dam, the Stanton 200 landslide blocked the Stanton River (fig. 61). Though somewhat smaller than the Leader 220 with a volume of 1,500,000 m^3, a source area of about 135,000 m^2, and a length of about 470 m (Massey and others, 2017), this landslide is very similar in style and geologic setting to the Leader 220. At the time of our fieldwork, it had impounded a lake a few hundred meters long in two pools connected by a small channel. This landslide is notable because just a small isthmus of the landslide deposits was damming these upper pools, and water was flowing over these deposits into much smaller and muddier pools (fig. 62), indicating that downcutting was occurring at the time of our last overflight on December 11, 2016. The Stanton 200 landslide also was covered by

Figure 58. Photograph showing the Leader 220 landslide dam. (See fig. 1*H*.)

Figure 59. Photograph showing the main scarp and head of the Leader 220 landslide. (See fig. 1*H*.)

Figure 60. Photograph showing the lake impounded by the Leader 220 landslide dam. (See fig. 1*H*.)

Figure 61. Photograph showing the Stanton 200 landslide dam and impounded lake. (See fig. 1*H*.)

coherent vegetation over most its surface and appears to be even less disrupted toward its toe than the Leader 220 landslide. Displacement from the crown to the top of the coherent vegetated deposits on the landslide head is about 50 m. Subsequent investigation shows that a strand of the Humps fault zone passes through the lower part of the landslide source area (Chris Massey, GNS Science, written commun., 2017).

No additional changes in the lake level were reported through March 2017, and clear water was flowing over the dam at that time (Environment Canterbury, 2017). Heavy rainfall from Cyclone Cook in April 2017 caused this landslide dam to breach. Debris from the dam extends about 500 m downstream onto a wide floodplain (Chris Massey, GNS Science, written commun., 2017).

Figure 62. Photograph showing water flow over the Stanton 200 landslide dam and ponding below the dam. (See fig. 1*H*.)

Mason 360 Landslide

The Mason 360 landslide (locally referred to as the Battery landslide) is a massive (approx. 2 km wide, 0.5 km long) preexisting landslide in Oligocene limestone and interspersed volcanic rocks. Fresh, incipient landslide blocks had partially detached from the main scarp, presumably from earthquake shaking, and fresh talus deposits were present along the base of most of the length of the main scarp and below minor cliffs in the sliding mass (fig. 63). Fresh cracking was visible on the body of the landslide in several places, but it is unclear if these cracks indicate local shallow deformation or reactivation of the entire mass along its basal shear surface. The Mason River, which flows through a canyon carved through the toe of the landslide, does not appear to be blocked or deflected by additional horizontal deep-seated sliding, with the exception of some small landslides off the steepened toe of the landslide. Post-earthquake interferometric synthetic aperture radar (InSAR) measurements suggest about 10 cm of movement on the main body of the landslide mass. Field measurements of displaced blocks near the landslide main scarp made by GNS Science after our visit show 0.5–1.0 m of displacement (Chris Massey, GNS Science, written commun., 2017).

Figure 63. Photograph showing the main scarp of the Mason 360 (Battery) landslide. (See fig. 1*H*.)

Other Landslides

The earthquake triggered numerous other landslides in this region; most are morphologically similar to the Leader 220 and Stanton 200 landslides, and many have very steep or vertical main scarps (figs. 64–68, see fig. 8). Many of the drainages in this region are small, so the water volumes impounded behind some of the dams were small at the time of our visit (see fig. 66). However, these impounded waters could become more hazardous when stream discharges increase or water transmission through or around the dams is impeded.

Mount Lyford

The steep gravel road that extends north from Mount Lyford to a ski resort was heavily damaged by ground failure, primarily slope-parallel cracking and spreading along the outboard edges (possibly formed in fill materials) of the mountainous road (see fig. 13). Several homes in Mount Lyford along the road to the resort were affected by localized ground failure, primarily ridgetop cracking (fig. 69). None of these features appeared to be large enough to affect multiple homes, nor did we see any signs of incipient large, deep slope failures from the steep mountains above the neighborhood.

Sea Cliffs

The steep sea cliffs south of Kaikoura and south of where State Highway 1 turns inland from the coast produced scattered shallow debris falls whose deposits are eroding rapidly under the influence of wave action (fig. 70). During our overflight, wave action was causing rapid erosion of the slide deposits, and offshore sediment plumes were visible along the shoreline. In some areas, the entire edge of the sea cliff failed, as indicated by lines of trees that toppled outward from the cliff face (fig. 71).

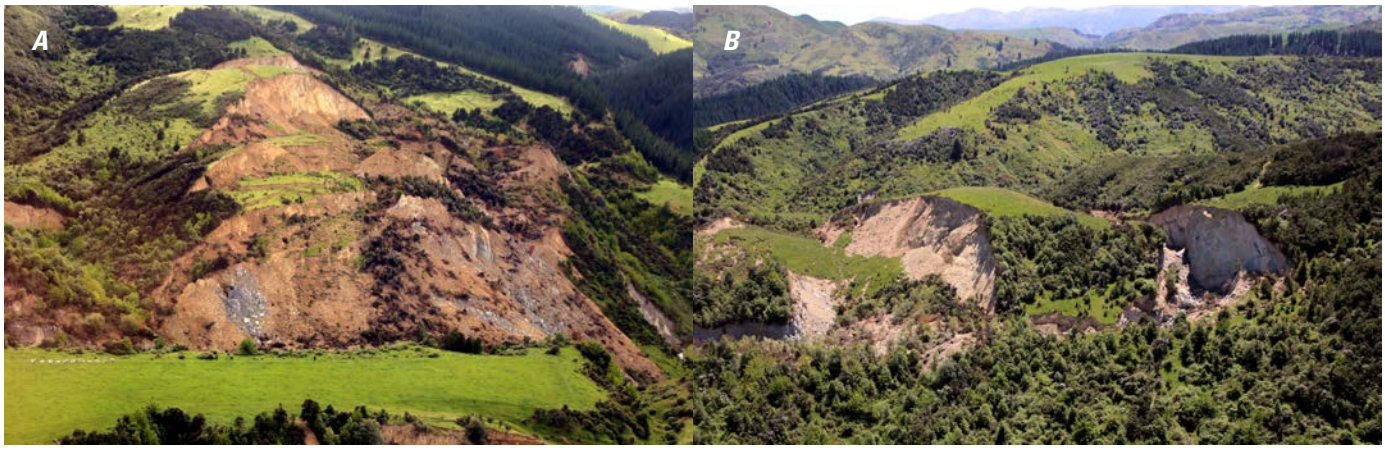

Figure 64. Photographs showing the Stanton East Tributary 170 landslide. *A*, Main body of the landslide consisting of several large, fairly coherent blocks. *B*, Nearly vertical main scarp and upper landslide blocks; landslide moved from right to left in photograph. (See fig. 1*H*.)

Figure 65. Photograph showing a landslide from the edge of the terrace directly across the valley from the Leader 220 landslide. (See fig. 1*H*.)

Figure 66. Photograph showing the Bourne 210 landslide. (See fig. 1*H*.)

Figure 67. Photograph showing the Bourne 270 landslide with a near-vertical headscarp. (See fig. 1*H*.)

Figure 68. Photograph showing a landslide between Waiau and Mount Lyford with a near-vertical headscarp. (See fig. 1*H*.)

Figure 69. Photograph showing a ridgetop crack extending through a house in Mount Lyford. (See fig. 1*G*.)

Figure 70. Photograph showing debris falls along coastal cliffs south of Kaikoura. (See fig. 1*B*.)

Figure 71. Photograph showing toppled trees along a section of sea cliff that failed south of Kaikoura. (See fig. 1*B*.)

Geologic Hazards Science Center
Publishing support provided by the Science Publishing Network,
Denver Publishing Service Center

For more information concerning the research in this report, contact the
Center Director, USGS Geologic Hazards Science Center
Box 25046, Mail Stop 966
Denver, CO 80225
(303) 273-8579

Or visit Geologic Hazards Science Center website at
https://geohazards.cr.usgs.gov/

ISSN 2328-0328 (online)
https://doi.org/10.3133/sir20175146